Supplementary Material (ESI) for Dalton Transactions
This journal is © The Royal Society of Chemistry

Highly efficient usage of hydrothermal technique through one-pot method to construct four Keggin-based compounds containing pendent ligands

Aixiang Tian,* Yali Ning, Jun Ying, Juwen Zhang, Xue Hou, Tianjiao Li, Xiuli Wang*

Department of Chemistry, Bohai University, Jinzhou 121000, P. R. China

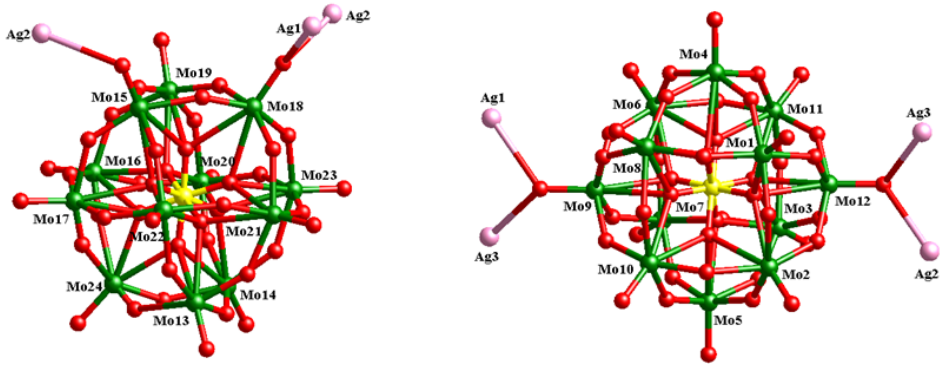

Mo13-containing PMo_{12} **Mo1-containing PMo_{12}**

Fig. S1. The three-connected Mo13-containing PMo_{12} anion and four-connected Mo1-containing PMo_{12} anion in compound **1**.

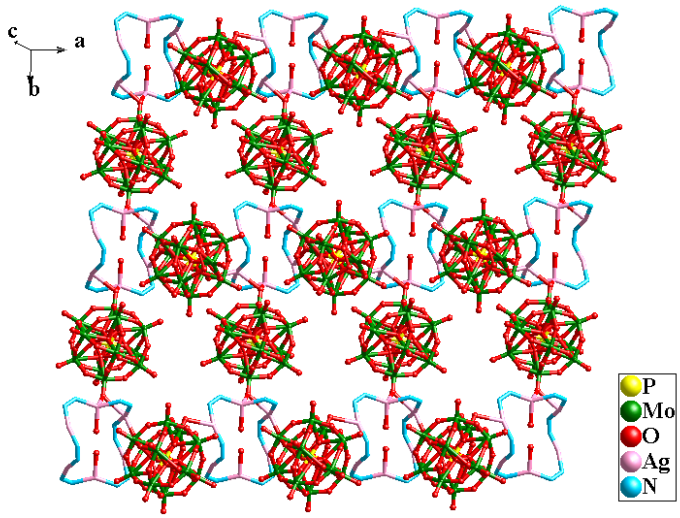

Fig. S2. The 2D layer of **1** with 1D chains linked by Mo1-containing PMo_{12} anions.

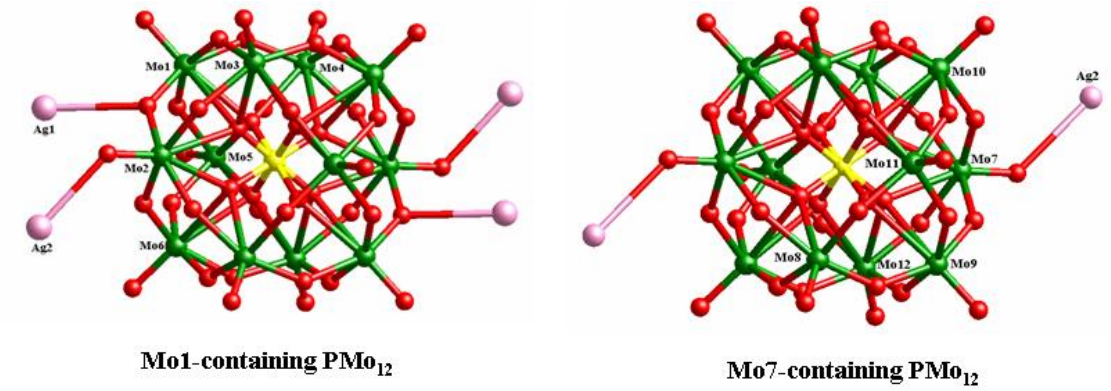

Fig. S3. The four-connected Mo1-containing PMo_{12} anion and two-connected Mo7-containing PMo_{12} anion in compound **2**.

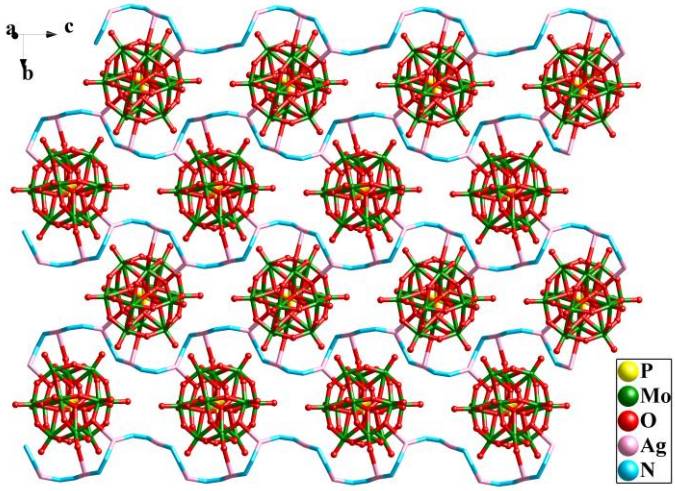

Fig. S4. The 2D layer of **2** with metal-organic chains linked by Mo1-containing PMo_{12} anions.

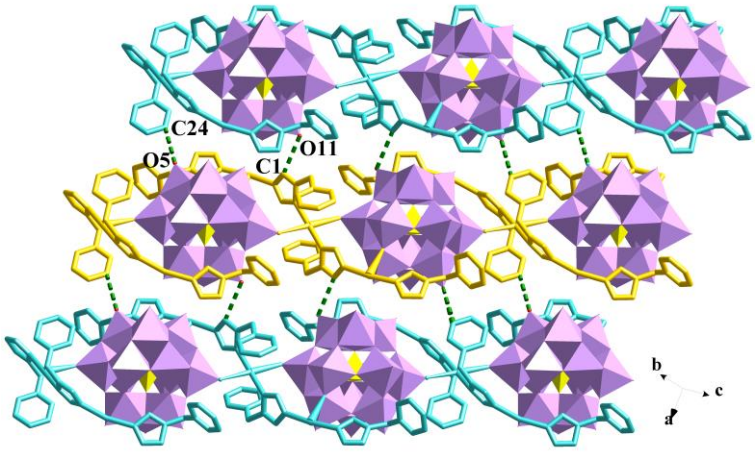

Fig. S5. The supramolecular layer of compound **3** with adjacent chains linked by hydrogen bonding interactions.

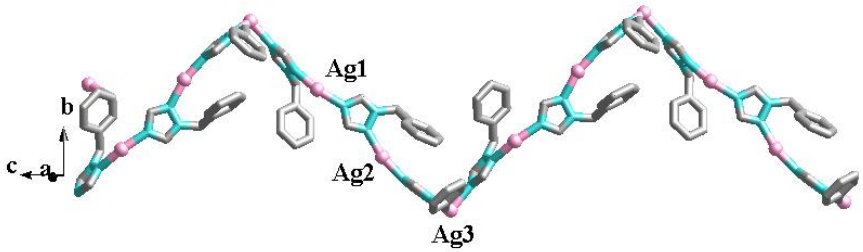

Fig. S6. The 1D zigzag metal-organic chain of compound **4**.

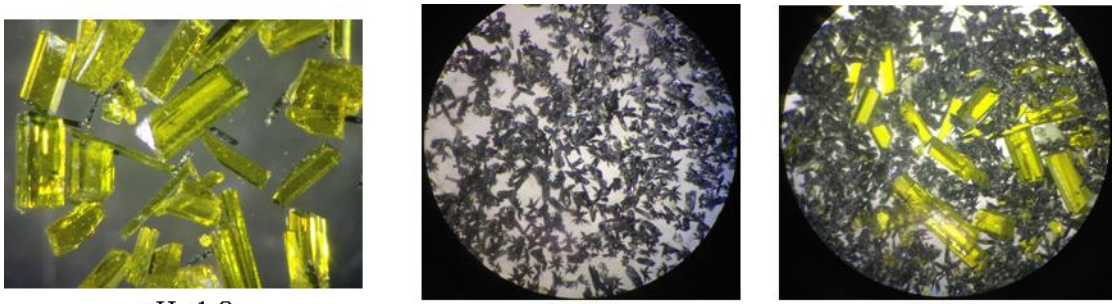

Fig. S7. The influence of pH on the yield of compounds **1** and **2**.

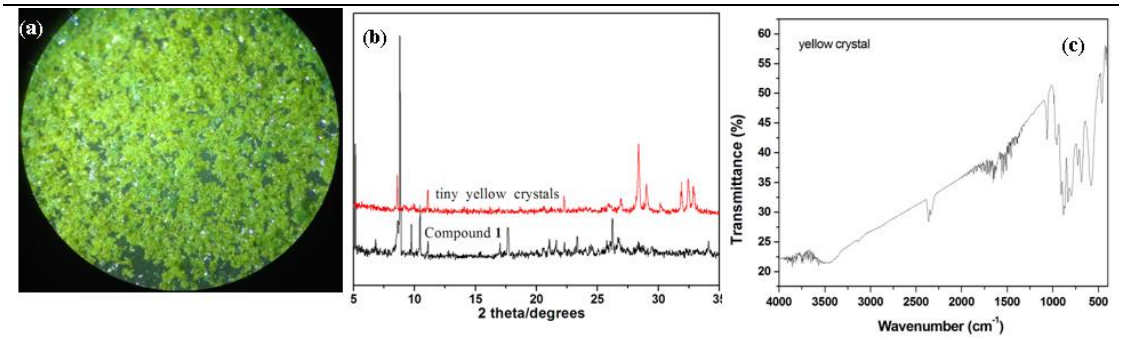

Fig. S8. The photo (a), XRD (b) and IR (c) of yellow crystals obtained below pH 1.8.

In the PMo_{12}-Ag-bpz system, when the pH is below 1.8, almost all of the product is tiny yellow crystals with high yield (Fig. S8a). We tried to check this compound by preliminary analysis. The yellow crystal is rather small to characterize by single crystal X-ray diffraction. Thus, we have performed FT-IR, XRD and ICP to preliminarily analyze these yellow crystals. The XRD (Fig. S8b) exhibits that the diffraction peaks of compound **1** and yellow crystal patterns don't match in positions, indicating that the yellow crystal is not compound **1**. The FT-IR spectrum (Fig. S8c) shows that the characteristic bands at 963, 880, 798 and 1062 cm^{-1} for yellow crystal are attributed to ν(Mo-O_t), ν(Mo-O_b-Mo), ν(Mo-O_c-Mo) and ν(P-O), respectively. Bands in the regions of 1656–1210 cm^{-1} are attributed to the bpz ligands. The IR spectrum shows that yellow crystals are based on PMo_{12}-bpz system. The ICP result shows that the Ag content is 8.17263 mg/L. Thus, the results mentioned above exhibit that yellow crystals are based on PMo_{12}-Ag-bpz system.

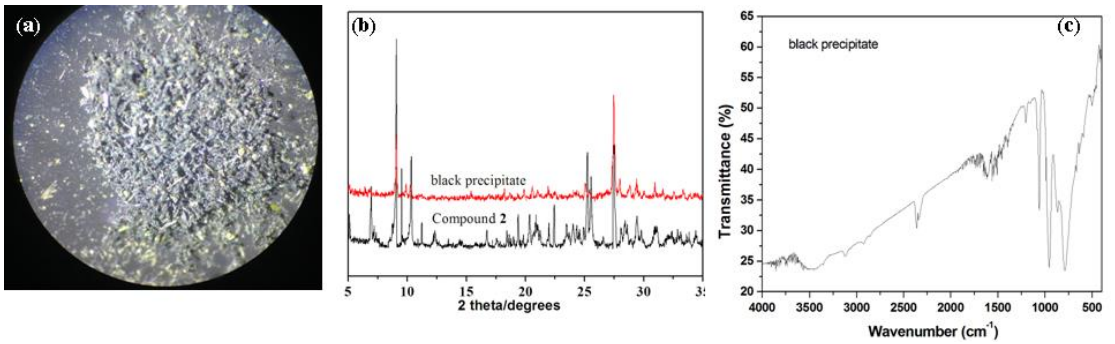

Fig. S9. The photo (a), XRD (b) and IR (c) of black precipitates obtained above pH 2.3 for PMo_{12}-Ag-bpz system.

Also in the PMo_{12}-Ag-bpz system, when the pH is above 2.3, almost all of the product is black precipitates with high yield (Fig. S9a). We tried to check this black precipitates by preliminary analysis. Thus, we have performed FT-IR and XRD to preliminarily analyze these black precipitates. The XRD (Fig. S9b) exhibits that the diffraction peaks of compound **2** and black precipitates patterns don't match in positions, indicating that the black precipitate is not compound **2**. The FT-IR spectrum (Fig. S9c) shows that the characteristic bands at 947, 875, 787 and 1057 cm^{-1} for black precipitates are attributed to ν(Mo-O_t), ν(Mo-O_b-Mo), ν(Mo-O_c-Mo) and ν(P-O), respectively. Bands in the regions of 1634–1200 cm^{-1} are attributed to the bpz ligands. Thus, the IR spectrum shows that black precipitates are also based on PMo_{12}-bpz system. The ICP result shows that the Ag content is 2.96698 mg/L. Thus, the results mentioned above exhibit that black precipitates are based on PMo_{12}-Ag-bpz system.

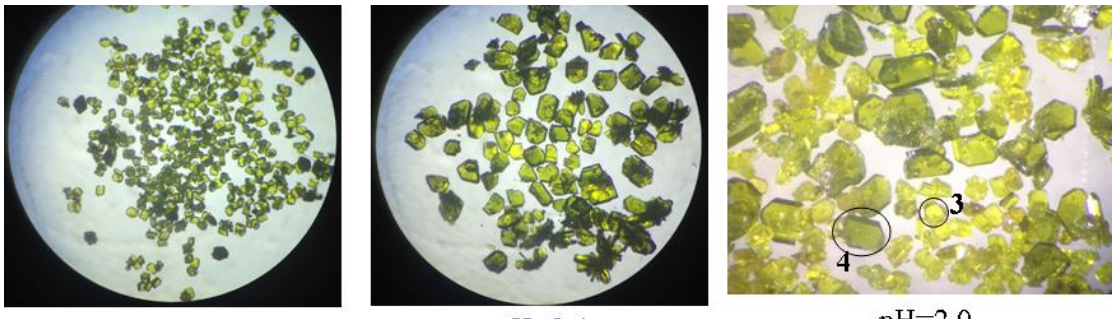

Fig. S10. The influence of pH on the yield of compounds **3** and **4**.

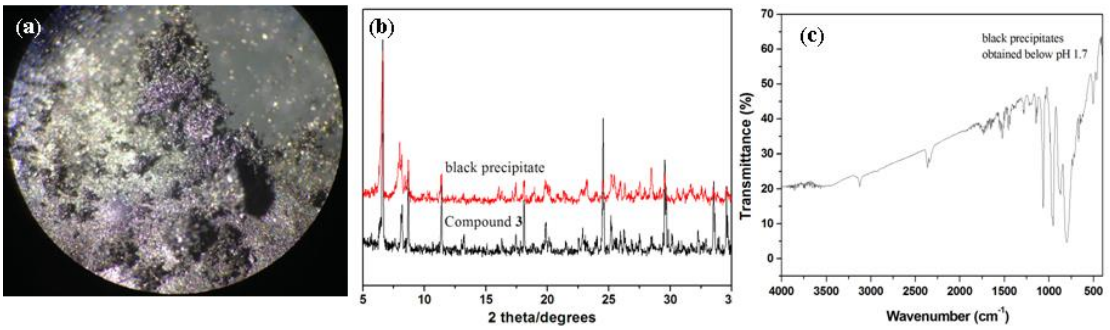

Fig. S11. The photo (a), XRD (b) and IR (c) of black precipitates obtained below pH 1.7 for PMo_{12}-Ag-btz system.

We also performed preliminary analysis to check black precipitates. In the PMo_{12}-Ag-btz system, when the pH is below 1.7, almost all of the product is black precipitates with high yield (Fig. S11a). Thus, we have performed FT-IR and XRD to preliminarily analyze the black precipitates obtained below pH 1.7. The XRD (Fig. S11b) exhibits that the diffraction peaks of compound **3** and black precipitate patterns match well in positions, indicating that the black precipitates obtained below pH 1.7 is the same as compound **3**, just with different states of aggregations. The FT-IR spectrum (Fig. S11c) further confirms this result. The characteristic bands at 957, 870, 798 and 1062 cm^{-1} for black precipitates are attributed to ν(Mo-O_t), ν(Mo-O_b-Mo), ν(Mo-O_c-Mo) and ν(P-O), respectively. Bands in the regions of 1727–1189 cm^{-1} are attributed to the btz ligands.

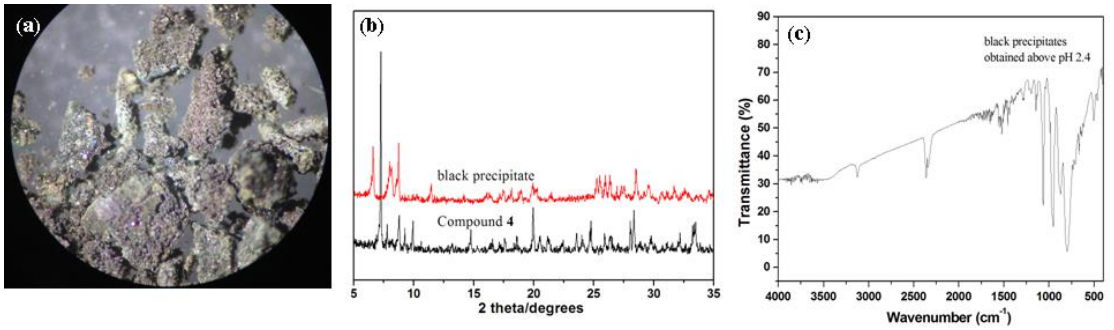

Fig. S12. The photo (a), XRD (b) and IR (c) of black precipitates obtained above pH 2.4 for PMo_{12}-Ag-btz system.

In the PMo_{12}-Ag-btz system, when the pH is above 2.4, almost all of the product is black precipitates with high yield (Fig. S12a). Thus, we have performed FT-IR and XRD to preliminarily analyze the black precipitates obtained above pH 2.4. The XRD (Fig. S12b) exhibits that the diffraction peaks of compound **4** and black precipitates patterns don't match in positions, indicating that the black precipitate obtained above pH 2.4 is not compound **4**. The FT-IR spectrum (Fig. S12c) shows that the characteristic bands at 952, 880, 793 and 1068 cm^{-1} for black precipitates are attributed to ν(Mo-O_t), ν(Mo-O_b-Mo), ν(Mo-O_c-Mo) and ν(P-O), respectively. Bands in the regions of 1650–1194 cm^{-1} are attributed to the btz ligands. Thus, the IR spectrum shows that black precipitates are also based on PMo_{12}-btz system. The ICP result shows that the Ag content is 0.677013 mg/L. Thus, the results mentioned above exhibit that black precipitates obtained above pH 2.4 are based on PMo_{12}-Ag-btz system.

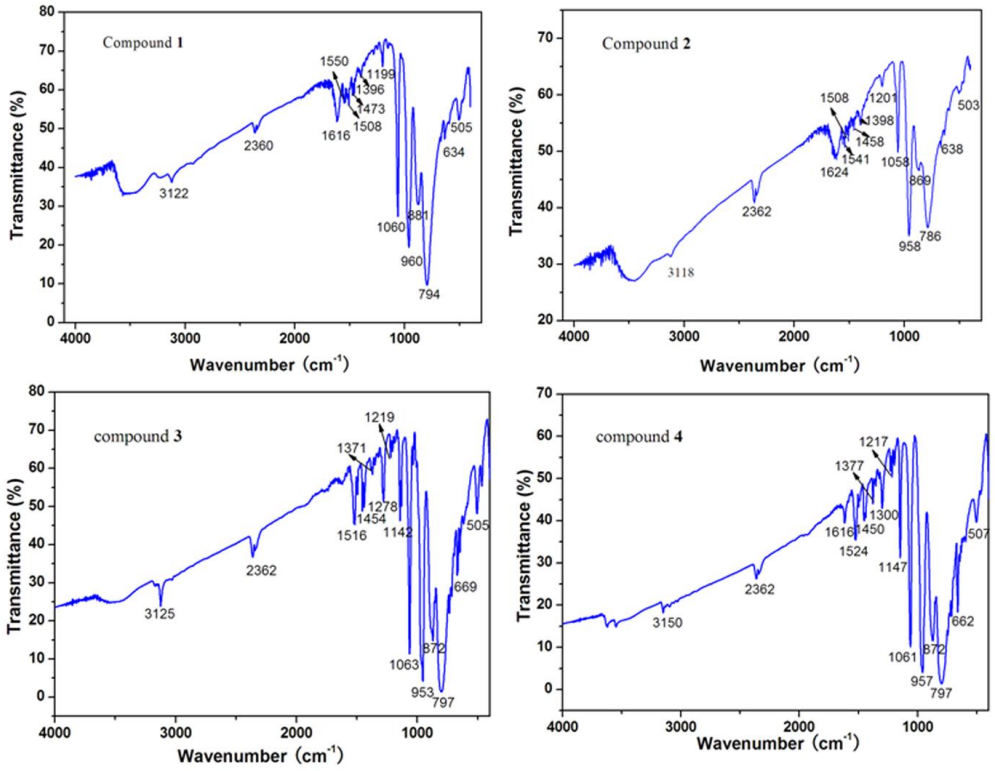

Fig. S13. The IR spectra of compounds **1**–**4**.

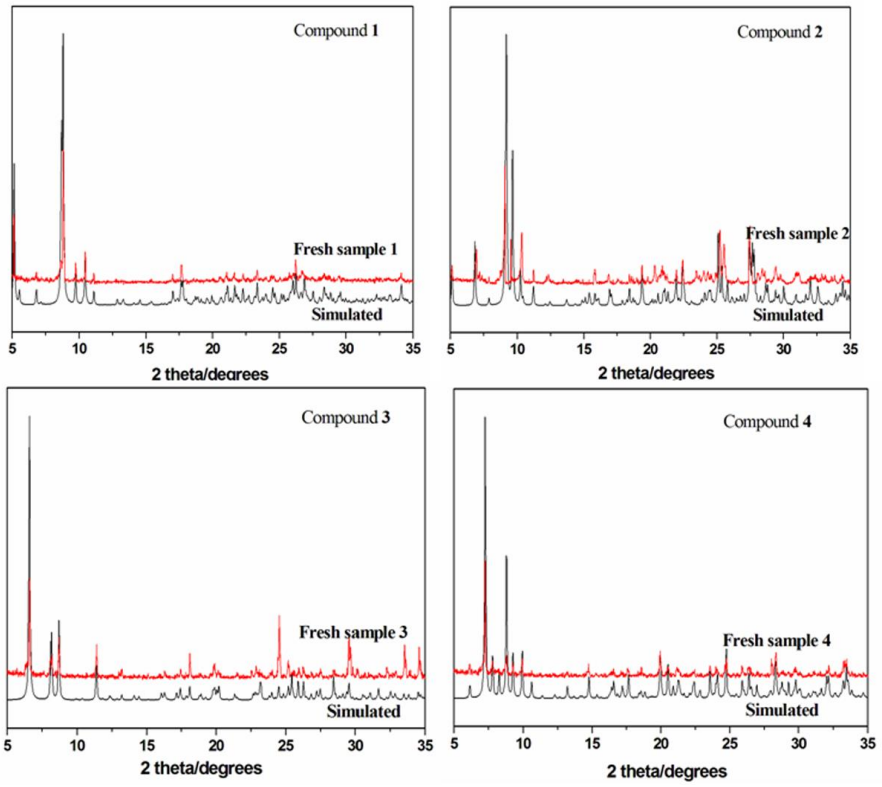

Fig. S14. The simulative (black line) and experimental (red line) powder X-ray diffraction patterns for compounds **1**–**4**.

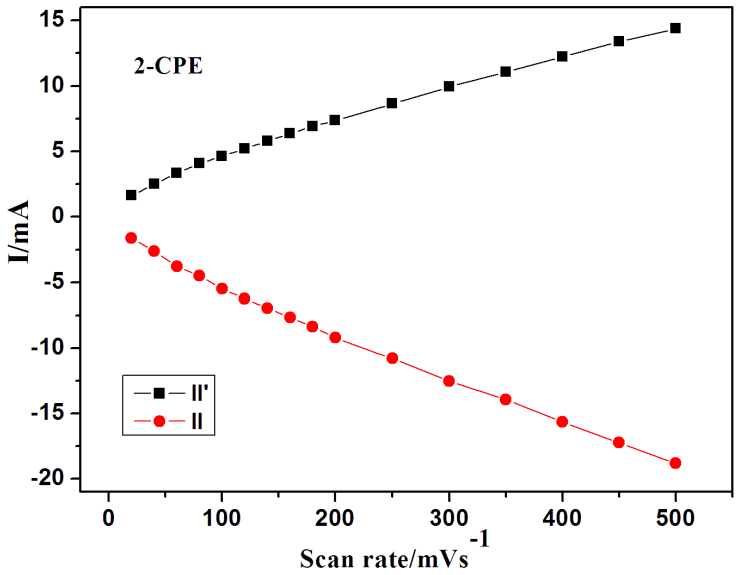

Fig. S15. The dependence of anodic peak (II) and cathodic peak (II') currents of **2**–CPE on scan rates.

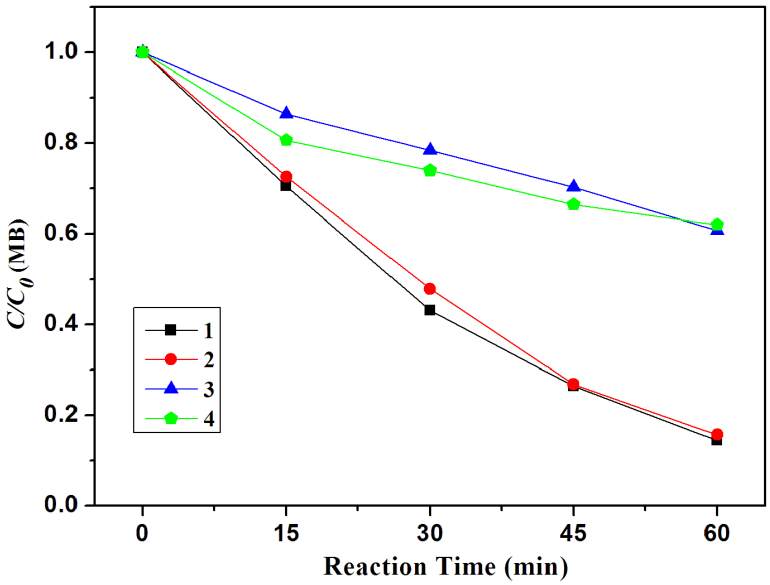

Fig. S16. Photocatalytic decomposition rate of the MB solution under UV irradiation with the use of the title compounds.

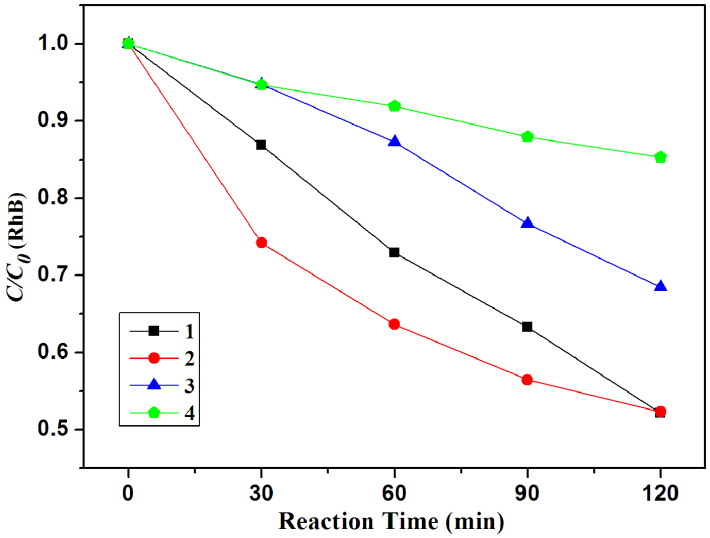

Fig. S17. Photocatalytic decomposition rate of the RhB solution under UV irradiation with the use of the title compounds.

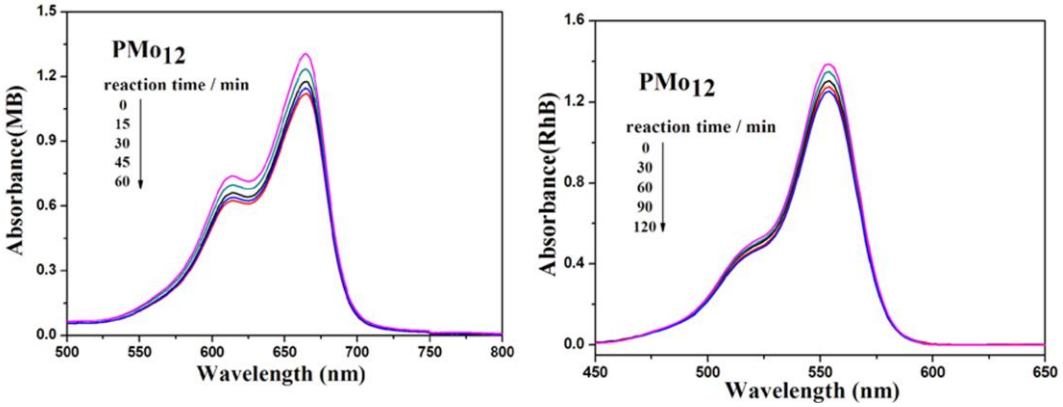

Fig. S18. Absorption spectra of the MB and RhB solution during the decomposition reaction under UV irradiation with the parent PMo_{12} as the catalyst.

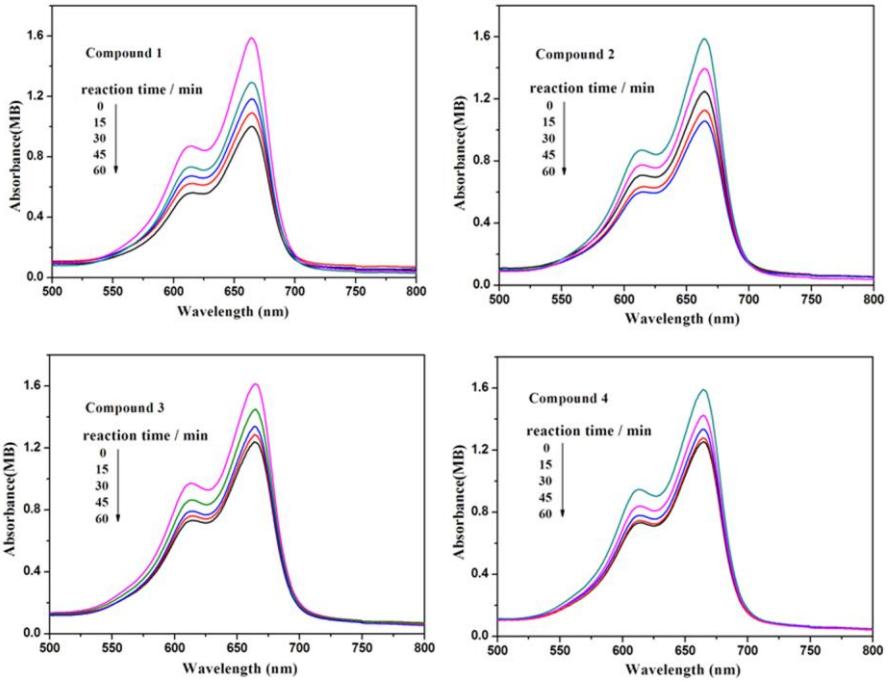

Fig. S19. Absorption spectra of the MB solution during the decomposition reaction in dark environment with the compounds **1–4** as the catalyst.

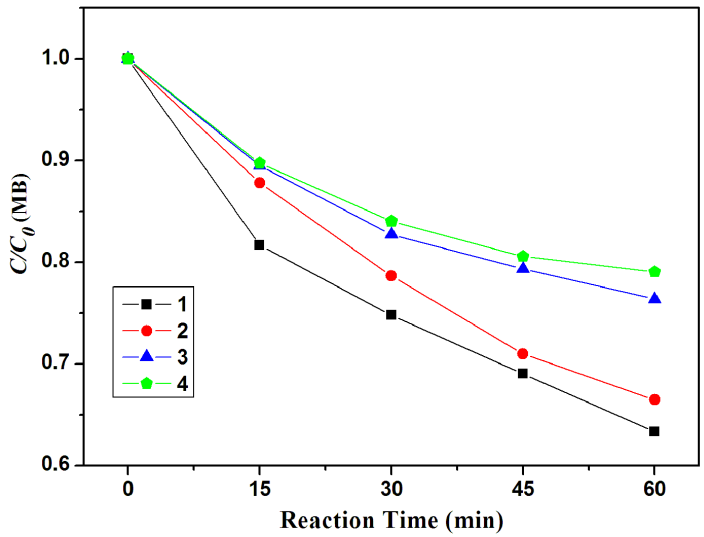

Fig. S20. Photocatalytic decomposition rate of the MB solution in dark environment with the use of the title compounds.

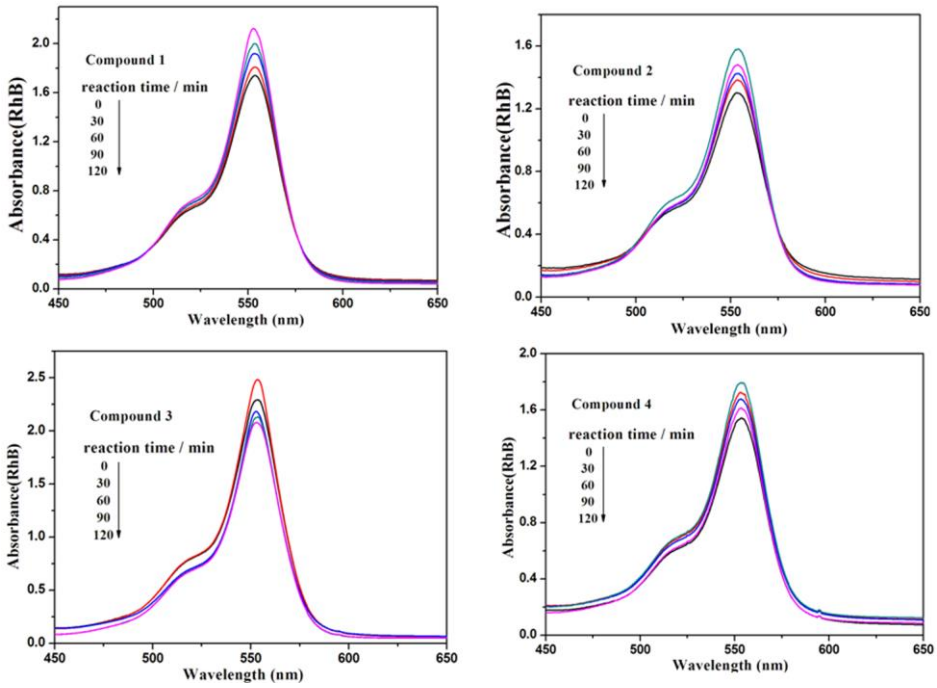

Fig. S21. Absorption spectra of the RhB solution during the decomposition reaction in dark environment with the compounds **1–4** as the catalyst.

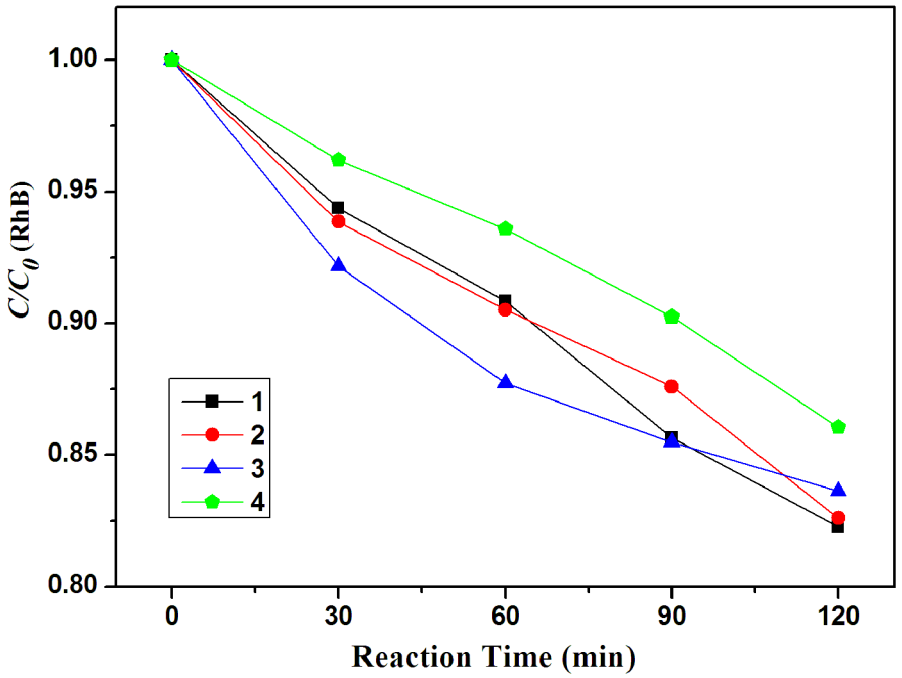

Fig. S22. Photocatalytic decomposition rate of the RhB solution in dark environment with the use of the title compounds.

Table S1. Selected bond distances (Å) and angles (deg) for compounds **1**–**4**.

compound **1**			
O(1W)-Ag(3)	2.389(17)	N(1)#1-Ag(2)-N(5)	165.2(5)
Ag(1)-N(6)	2.158(15)	C(1)-N(1)-Ag(2)#1	131.9(12)
Ag(1)-N(3)	2.158(14)	N(6)-N(5)-Ag(2)	128.5(11)
Ag(2)-N(1)#1	2.168(15)	C(17)-N(5)-Ag(2)	124.6(12)
Ag(2)-N(5)	2.181(14)	N(2)-N(1)-Ag(2)#1	121.1(11)
N(1)-Ag(2)#1	2.168(15)	N(2)-Ag(3)-N(4)	146.6(5)
Ag(3)-N(2)	2.213(16)	N(2)-Ag(3)-O(1W)	105.4(6)
Ag(3)-N(4)	2.230(15)	N(4)-Ag(3)-O(1W)	108.0(6)
N(4)-N(3)-Ag(1)	121.6(11)	C(3)-N(2)-Ag(3)	130.7(13)
N(3)-Ag(1)-N(6)	166.3(6)	N(1)-N(2)-Ag(3)	121.2(11)
C(15)-N(6)-Ag(1)	129.2(15)	C(8)-N(4)-Ag(3)	131.3(13)
N(5)-N(6)-Ag(1)	126.5(11)	N(3)-N(4)-Ag(3)	120.6(11)
C(10)-N(3)-Ag(1)	131.1(12)		
Symmetry transformations used to generate equivalent atoms for **1**: #1 -x+2,-y+1,-z+1			
compound **2**			
Ag(1)-N(1)	2.179(10)	N(2)-N(1)-Ag(1)	128.6(8)
Ag(1)-N(3)	2.174(10)	C(8)-N(2)-Ag(2)	127.0(9)
Ag(2)-N(4)#3	2.186(9)	N(1)-N(2)-Ag(2)	125.3(8)
Ag(2)-N(2)	2.195(10)	C(1)-N(3)-Ag(1)	123.8(8)
N(4)-Ag(2)#4	2.186(9)	N(4)-N(3)-Ag(1)	129.6(7)
N(3)-Ag(1)-N(1)	138.0(4)	C(3)-N(4)-Ag(2)#4	125.1(8)
N(4)#3-Ag(2)-N(2)	170.7(4)	C(10)-N(1)-Ag(1)	119.5(10)
N(3)-N(4)-Ag(2)#4	127.9(7)		
Symmetry transformations used to generate equivalent atoms for **2**: #3 x,-y-3/2,z-1/2; #4 x,-y-3/2,z+1/2			
compound **3**			
Ag(1)-N(4)	2.148(4)	Ag(3)-N(8)	2.294(4)
Ag(2)-N(3)#1	2.277(4)	Ag(4)-N(7)	2.119(4)
Ag(2)-N(3)	2.277(4)	Ag(3)-N(8)#2	2.294(4)
Ag(1)-N(1)	2.160(4)	Ag(3)-O(7)#2	2.415(3)
Ag(2)-O(14)	2.527(3)	Ag(3)-O(7)	2.415(3)
Ag(2)-O(14)#1	2.527(3)	Ag(4)-N(10)	2.123(4)
N(4)-Ag(1)-N(1)	170.46(17)	N(3)#1-Ag(2)-N(3)	179.999(2)
C(1)-N(1)-Ag(1)	124.1(4)	N(8)-Ag(3)-N(8)#2	179.999(2)
N(3)#1-Ag(2)-O(14)#1	93.52(13)	N(8)-Ag(3)-O(7)#2	88.94(13)
C(2)-N(1)-Ag(1)	131.2(4)	N(8)#2-Ag(3)-O(7)#2	91.06(13)
N(3)-Ag(2)-O(14)#1	86.48(13)	N(3)#1-Ag(2)-O(14)	86.48(13)
N(3)-Ag(2)-O(14)	93.52(13)	N(8)#2-Ag(3)-O(7)	88.94(13)
O(14)#1-Ag(2)-O(14)	179.998(1)	O(7)#2-Ag(3)-O(7)	180.00(16)
N(8)-Ag(3)-O(7)	91.06(13)	C(19)-N(7)-Ag(4)	129.2(4)
C(2)-N(3)-Ag(2)	135.4(4)	C(11)-N(4)-Ag(1)	124.2(3)
N(7)-Ag(4)-N(10)	167.36(19)	C(10)-N(4)-Ag(1)	131.9(4)

N(2)-N(3)-Ag(2)	117.9(4)	C(20)-N(7)-Ag(4)	126.0(4)
Mo(1)-O(7)-Ag(3)	162.8(2)	N(9)-N(8)-Ag(3)	118.9(3)
C(19)-N(8)-Ag(3)	135.3(4)	Mo(2)-O(14)-Ag(2)	136.91(18)
C(28)-N(10)-Ag(4)	132.5(4)	C(29)-N(10)-Ag(4)	123.8(4)
Symmetry transformations used to generate equivalent atoms for **3**: #1 -x+1,-y+1,-z+1; #2 -x,-y,-z+2			
Compound **4**			
O(8)-Ag(1)	2.586(7)	C(10)-N(6)-Ag(2)	132.8(6)
Ag(1)-N(4)	2.145(7)	N(5)-N(6)-Ag(2)	123.3(5)
Ag(1)-N(3)	2.169(7)	Ag(3)-N(1)	2.251(8)
Ag(2)-N(6)	2.136(6)	N(9)-Ag(3)#4	2.307(7)
Ag(2)-N(7)	2.105(7)	Ag(3)-N(9)#1	2.307(7)
N(4)-Ag(1)-N(3)	156.6(3)	Ag(3)-C(8)#2	2.535(10)
Mo(8)-O(8)-Ag(1)	137.2(4)	C(8)-Ag(3)#3	2.535(10)
N(3)-Ag(1)-O(8)	92.9(2)	C(1)-N(1)-Ag(3)	126.4(6)
N(2)-N(3)-Ag(1)	120.8(6)	C(2)-N(1)-Ag(3)	129.8(7)
C(2)-N(3)-Ag(1)	135.3(6)	N(1)-Ag(3)-C(8)#2	126.3(4)
C(11)-N(4)-Ag(1)	124.3(5)	C(20)-N(9)-Ag(3)#4	125.0(6)
C(10)-N(4)-Ag(1)	132.3(6)	N(9)#1-Ag(3)-C(8)#2	101.0(3)
C(19)-N(7)-Ag(2)	128.5(6)	N(1)-Ag(3)-N(9)#1	99.9(3)
N(7)-Ag(2)-N(6)	166.3(3)	N(8)-N(9)-Ag(3)#4	129.8(5)
C(20)-N(7)-Ag(2)	126.9(6)		
Symmetry transformations used to generate equivalent atoms for **4**: #1 x-1/2,-y+1/2,z-1/2; #2 -x+1/2,y+1/2,-z+1/2; #3 -x+1/2,y-1/2,-z+1/2; #4 x+1/2,-y+1/2,z+1/2			